IDŐJÁRÁS

Quarterly Journal of the Hungarian Meteorological Service
Vol. 119, No. 3, July – September, 2015, pp. 379–398

Combined closure single-column atmospheric boundary layer model

Árpád Bordás* and **Tamás Weidinger**

Department of Meteorology, Eötvös Loránd University,
P.O. Box 32, H-1518 Budapest, Hungary;

**Corresponding author E-mail: abordas@caesar.elte.hu*

(Manuscript received in final form March 20, 2015)

Abstract—This paper presents a development of the first order combined closure (local and nonlocal) single-column atmospheric boundary layer model. The model simulates the turbulent mixing of sensible heat, moisture, and momentum as a split between small scale (subgrid) and large scale (supergrid) processes according to the estimated ratio between local and nonlocal mixing. To verify the validity of the model, an evaluation process was conducted. The evaluation process included controlled offline numerical experiments and tests using the Wangara Experiment database. The obtained vertical profiles and estimated boundary layer heights are in good agreement with the Wangara observation data. Furthermore, uncertainty range affected by the choice of profile functions when estimating the ratio between local and nonlocal mixing processes was analyzed.

Key-worlds: atmospheric boundary layer, turbulent mixing, single-column model, combined (local and nonlocal) approach, Wangara Experiment

1. Introduction

Almost all human and biological activities take place in the atmospheric boundary layer (ABL), where the direct effects of the Earth's surface are noticeable. Therefore, the description of the boundary layer characteristics as well as the simulation of the turbulent mixing processes in the ABL are important for weather prediction, air pollution, and environmental modeling. When neglecting horizontal advection, the governing ABL equations in single-column (1D) form for the northern hemisphere are:

$$\frac{\partial \theta}{\partial t} = -\frac{\partial\left(\overline{w'\theta'}\right)}{\partial z}, \tag{1}$$

$$\frac{\partial q}{\partial t} = -\frac{\partial\left(\overline{w'q'}\right)}{\partial z}, \tag{2}$$

$$\frac{\partial u}{\partial t} = f\left(v - v_g\right) - \frac{\partial\left(\overline{u'w'}\right)}{\partial z}, \tag{3}$$

$$\frac{\partial v}{\partial t} = -f\left(u - u_g\right) - \frac{\partial\left(\overline{v'w'}\right)}{\partial z}, \tag{4}$$

where θ is the potential temperature, q is the specific humidity, u and v are the horizontal wind velocity components, u_g and v_g are the corresponding geostrophic wind components, $\overline{w'\theta'}$, $\overline{w'q'}$, $\overline{u'w'}$, and $\overline{v'w'}$ represent vertical fluxes, f denotes the Coriolis parameter, and z is the vertical coordinate.

Single-column ABL models differ in the main mixing assumption and the approach to the closure problem (*Stull*, 1988; *Foken*, 2006). The choice of a model depends on the aim of investigation and on the modelers' conception. Assuming that the turbulence is analogous to molecular diffusion, different types of first and higher order local closure procedures were developed. This approach is reasonable during conditions of stable and neutral static stability, when the scale of turbulent motion is much smaller than the scale of mean motion. In the convective ABL, where the boundary layer is directly affected by the solar heating of the surface, much of the mixing is caused by buoyant plumes originating in the surface layer and rising to the top of the boundary layer. When using nonlocal mixing schemes (*Blackadar* 1978; *Zhang* and *Anthes*, 1982; *Fiedler* and *Moeng*, 1985), the effects of local mixing during convective conditions are neglected and turbulent mixing is simulated by different size discrete convective elements. To simulate both local (small scale) and nonlocal (large scale) mixing processes simultaneously, combined closure (local and nonlocal) mixing schemes (*Stull*, 1984; *Pleim* and *Chang*, 1992 *Pleim*, 2007a; *Bordás*, 2008) were developed.

Single-column models are very useful tools in ABL investigation. Such models are comprehensive enough to illustrate basic ABL characteristics, simulate boundary layer processes (*Holtslag* and *Boville*, 1993), and compare different parameterization processes (*Alapaty et al.*, 1997; *Bosveld et al.*, 2014). Nesting 1D models in 3D environment, such as MM5 (*Berg* and *Zhong*, 2005; *Pleim*, 2007b) and WRF (*Hu et al.*, 2010; *Shin* and *Hong*, 2011; *Xie et al.*, 2012; *Kleczek et al.*, 2014), we can provide detailed and accurate information of the ABL structure.

The aim of our study is to represent the designed first order single-column ABL model (mixing concept, calculation of turbulent mixing rates, and estimation of the ABL height), which employs a combined (local and nonlocal) mixing scheme, as well as to introduce the model evaluation process done by controlled offline numerical experiments and the Wangara Experiment database. In stable and neutral static conditions, turbulent mixing is simulated as a subgrid (local) process. In unstable conditions, depending on the calculated ratio between local and nonlocal mixing of heat, the model simulates turbulent mixing of sensible heat, moisture, and momentum as a split between small scale and large scale processes. In addition, we analyzed how the type of profile function affected the uncertainty range when estimating the local versus nonlocal character of the turbulent mixing.

2. Estimation of the local to nonlocal mixing ratio

For the combined modeling of the boundary layer processes, it is necessary to define the explicit local and nonlocal vertical fluxes. Many ABL models (*Troen* and *Mahrt*, 1986; *Holtslag* and *Boville*, 1993; *Noh et al.* 2003, *Hong et al.*, 2006) simulate the nonlocal mixing of the different prognostic variables (*c*; θ, *q*, *u*, *v*) including gradient adjustment term (γ_c) into eddy diffusivity equation as:

$$-\frac{\partial\left(\overline{w'c'}\right)}{\partial z}=\frac{\partial}{\partial z}\left[K_c\left(\frac{\partial c}{\partial z}-\gamma_c\right)\right], \tag{5}$$

where K_c denotes the vertical eddy diffusivity for the quantity of interest. The gradient adjustment term, representing nonlocal influences on the turbulent mixing, can be estimated as (*Holtslag* and *Boville*, 1993):

$$\gamma_c = a\frac{w_*\left(\overline{w'c'}\right)_0}{w_m^2 h}, \tag{6}$$

where $\left(\overline{w'c'}\right)_0$ is the surface kinematic flux of the transported variable, w_* represents the convective velocity scale, $w_m = u_*/\Phi_m$ (where u_* is the friction velocity and Φ_m denotes the profile function for momentum), *h* denotes the height of the boundary layer, and *a* is a semi-empirical constant. Under neutral static conditions for which $w_* = 0$, the gradient adjustment term vanishes. This approach is most valid for heat, since surface heat flux is the source and driver of convective turbulence. For other quantities, the surface heat flux is replaced by the surface flux of the transported quantity. However, nonlocal effects may

be driven by mechanisms completely unrelated to convective turbulence. For quantities that have no upward surface fluxes, these models revert to the local eddy diffusivity model.

Following *Pleim* (2007a) from Eq. (5), we can define the ratio between local and nonlocal heat mixing fluxes (R) as:

$$R = \frac{K_h \left| \partial\theta / \partial z \right|}{K_h \gamma_h}. \tag{7}$$

When estimating this ratio, it is possible to obtain information about the physical characteristics of the convective boundary layer applicable to any prognostic variable. The surface sensible heat flux can be approximated as:

$$\left(\overline{w'\theta'}\right)_0 = -\kappa \frac{u_* z_s}{\Phi_h} \frac{\partial\theta}{\partial z}, \tag{8}$$

where z_s is the thickness of the surface layer ($z_s = 0.1h$), and Φ_h denotes the profile function for heat. The convective velocity scale, defined by *Troen* and *Mahrt* (1986) as $w_* = \left[\beta \left(\overline{w'\theta_v'}\right)_0 h\right]^{1/3}$, is estimated in the form:

$$w_* = u_* \kappa^{-\frac{1}{3}} \left(-\frac{h}{L}\right)^{\frac{1}{3}}, \tag{9}$$

where L represents the Monin-Obukhov length scale, and κ is the von Kármán constant. The Monin-Obukhov length scale is calculated as:

$$L = -\frac{u_*^3}{\beta \kappa \left(\overline{w'\theta'}\right)_0}, \tag{10}$$

where β denotes the buoyancy parameter ($\beta = g / T_0$, g is the acceleration due to gravity, and T_0 is the average temperature in the surface layer). According to Eq. (6) to Eq. (10), the ratio between local and nonlocal mixing can be expressed as:

$$R = \left[0.1a\kappa^{\frac{2}{3}} \left(-\frac{h}{L}\right)^{\frac{1}{3}} \frac{\Phi_m^2}{\Phi_h} \right]^{-1}. \tag{11}$$

It can also be linked to the ratio of the nonlocal flux to the total flux (f_{conv}), defined by *Pleim* (2007a), as:

$$f_{conv} = \frac{1}{R+1}. \tag{12}$$

The local versus nonlocal turbulent mixing ratio (R) defined by Eq. (11) behaves as a function of stability ($-h/L$) and depends on the choice of profile functions for momentum and heat (Φ_m^2/Φ_h). Comparing different profile functions, we can analyze the uncertainty caused by the choice of profile functions. *Table 1* lists four often used profile functions for unstable stratification, intervals of definition, and the von Kármán constant used by different authors. The detailed comparison of the profile functions for both stable and unstable conditions, as well as the effects of uncertainties on the calculation of surface layer fluxes are provided by *Weidinger et al.* (2000), *Ács* and *Kovács* (2001), *Arya* (2001), and *Kramm et al.* (2013). *Fig. 1* illustrates how Φ_m^2/Φ_h, obtained by the listed profile functions, depends as a function of non-dimensional height (z/L). For *Dyer*'s (1974) profile functions, Φ_m^2/Φ_h equals 1 throughout the interval of definition ($-1 \le z/L \le 0$). When using the *Businger et al.* (1971) functions, Φ_m^2/Φ_h is greater than 1, while when applying the *Dyer* and *Bradley* (1982) functions, Φ_m^2/Φ_h is smaller than 1. For both universal function types, Φ_m^2/Φ_h is decreasing about 30% in the first part of the considered interval of definition ($-1 \le z/L \le 0$) and is nearly constant in the second part of the considered interval ($-2 \le z/L \le -1$). For the *Zilitinkevich* and *Chalikov* (1968) functions, Φ_m^2/Φ_h is decreasing rapidly in the total interval of definition ($-1.2 \le z/L \le 0$).

As the aim of the subsequent analysis was to determine whether and to what extent the choice of profile function type influenced the uncertainty range, we used the *Dyer*-type profile functions for which Φ_m^2/Φ_h equals 1 in the interval of definition, and set the von Kármán constant to 0.41. The semi-empirical constant a (see Eq. (6) and Eq. (11)) was set to 7.2 (*Holtslag* and *Boville*, 1993). *Fig. 2* shows how the ratio between local to nonlocal mixing processes (R) behaves as a function of stability. To estimate the uncertainty range caused by using different profile functions, the value of the semi-empirical constant a was varied by ± 15% and ± 25%. The obtained results are also presented in *Fig. 2*. For $R = 1$, the local and nonlocal mixing processes are in balance. When the value is higher than 1, it is the local processes that dominate, while when the value is lower than 1, it is the nonlocal processes that prevail. Due to the inverse proportion between R and a, when the value of the semi empirical constant is increasing, the effects of local mixing processes are decreasing. Nonlocal processes became dominant for very unstable conditions ($-h/L > 10$). During extremely convective conditions ($-h/L = 30$), the value of R is not lower than 0.65. Our results verify the combined mixing range of the unstable ABL. The uncertainty range is not significantly affected by the choice of profile function type in estimation of the ratio between local versus nonlocal mixing.

Table 1. Some frequently used profile functions in the case of unstable stratification,

intervals of definition, and estimation of the von Kármán constant

	profile function	interval	*k*
Zilitinkevich and *Chalikov* (1968)	$\Phi_m = \Phi_h = 1 + 1.45\frac{z}{L}$ $\Phi_m = \Phi_h = 0.417\left(-\frac{z}{L}\right)^{-\frac{1}{3}}$	$-0.16 \le \frac{z}{L} \le 0$ $-1.2 \le \frac{z}{L} \le -0.16$	0.43
Businger et al. (1971)	$\Phi_m = \left(1-15\frac{z}{L}\right)^{-\frac{1}{4}}$ $\Phi_h = 0.74\left(1-9\frac{z}{L}\right)^{-\frac{1}{2}}$	$-2 \le \frac{z}{L} \le 0$	0.35
Dyer (1974)	$\Phi_m = \left(1-16\frac{z}{L}\right)^{-\frac{1}{4}}$ $\Phi_h = \left(1-16\frac{z}{L}\right)^{-\frac{1}{2}}$	$-1 \le \frac{z}{L} \le 0$	0.41
Dyer and *Bradley* (1982)	$\Phi_m = \left(1-28\frac{z}{L}\right)^{-\frac{1}{4}}$ $\Phi_h = \left(1-14\frac{z}{L}\right)^{-\frac{1}{2}}$	$-4 \le \frac{z}{L} \le 0$	0.4

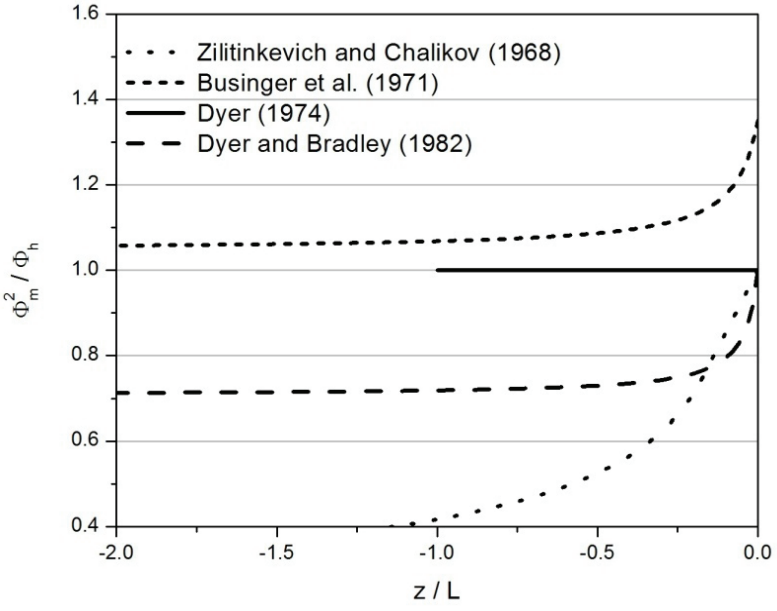

Fig. 1. Φ_m^2 / Φ_h as a function of non-dimensional height (z/L) using different universal functions.

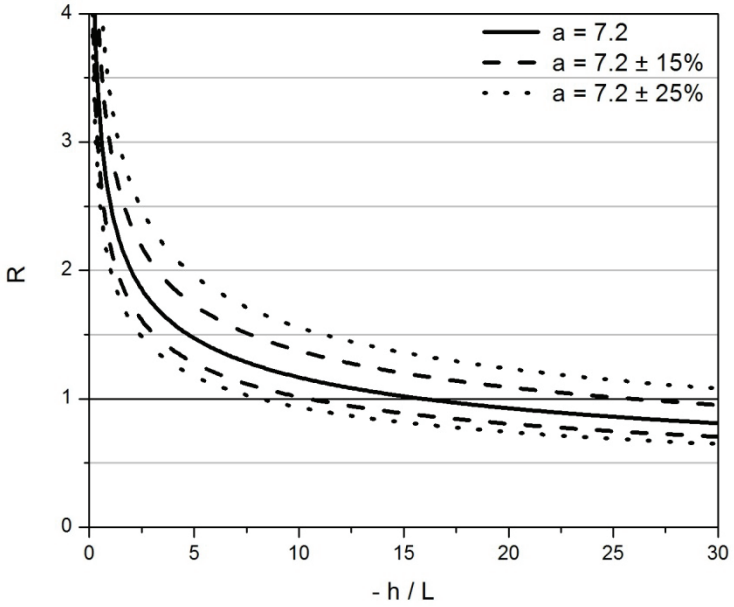

Fig. 2. The ratio between local and nonlocal turbulent mixing processes (*R*) as a function of stability.

3. Model description

3.1. Mixing concept

The model designed by the authors describes turbulent mixing during stable and neutral static conditions employing the standard eddy diffusion scheme. For unstable conditions, the model calculates the ratio between local and nonlocal mixing processes (*R*, defined by Eq. (11)) in every time step. According to the calculated ratio, turbulent mixing of sensible heat, moisture, and momentum are simulated as a split between local and nonlocal mixing processes employing a combined (local and nonlocal) closure mixing scheme (*Bordás*, 2008). Stability is defined by the bulk Richardson number method for the lowest model layer. The inclusion of the nonlocal mixing components of momentum can provide more realistic wind profiles for unstable conditions (*Frech* and *Mahrt*, 1995 *Brown* and *Grant*, 1997). However, it is not yet clear how the inclusion of the nonlocal mixing of momentum can improve general properties of a boundary layer model (*Noh et al.*, 2003).

The mixing scheme (*Bordás*, 2008) used for simulating turbulent mixing during unstable conditions combines the local eddy diffusion scheme and the nonlocal Blackadar scheme (*Blackadar,* 1978). The Blackadar scheme describes nonlocal mixing, transporting material directly from the lowest model layer to every other layer and symmetrically from each layer back to the surface layer as it is shown in *Fig. 3*. The explicit value of nonlocal exchange of the prognostic variable at layer *i* can be calculated as $M(c_1 - c_i)$, where M [s^{-1}] is the convective

mixing rate. Such a model was applied as one of the mixing schemes in MM4 (*Zhang* and *Anthes*, 1982) and MM5 (*Zhang* and *Zheng*, 2004; *Berg* and *Zhong*, 2005) models to simulate boundary layer processes during free convection.

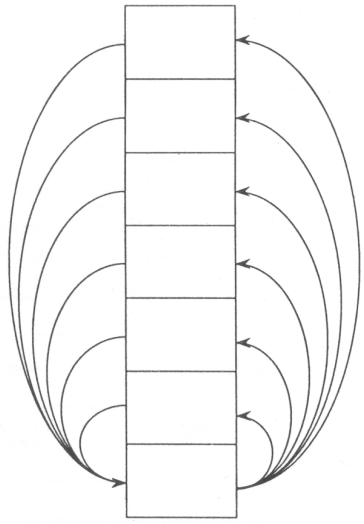

Fig. 3. Schematic representation of the Blackadar mixing scheme.

Since the total mixing is simulated as a split between local and nonlocal mixing components, we estimate the weighted vertical eddy diffusivity for heat and momentum (K'_{hm}) and the weighted upward mixing rate (M') as:

$$K'_{hm} = \frac{R}{R+1} K_{hm} = (1 - f_{conv}) K_{hm} , \tag{13}$$

and

$$M' = \frac{1}{R+1} M = f_{conv} M . \tag{14}$$

At either extremes ($R \to \infty$ or $R = 0$), the mixing reverts to the simple eddy diffusivity scheme and Blackadar scheme, respectively.

3.2. Calculation of the vertical eddy diffusivity and convective mixing rate

The model defines vertical eddy diffusivity for heat and momentum (K_{hm}) by boundary layer scaling, similarly to *Hotlsag* and *Boville* (1993) as:

$$K_{hm}(z) = \kappa \frac{u_* z}{\Phi_{hm}(z/L)} \left(1 - \frac{z}{h}\right)^2, \tag{15}$$

where Φ_{hm} is the corresponding profile function. The convective mixing rate (M) used for any prognostic variable was calculated according to *Pleim* (2007a) as:

$$M = -\frac{1}{h - z_1} \frac{F_{h1}}{\theta_v(z_2) - \theta_v(z_1)}, \tag{16}$$

where F_{h1} is the sensible heat flux in the lowest model layer, $\theta_v(z_2)$ and $\theta_v(z_1)$ represent the virtual potential temperature at the top and bottom of the lowest model layer, respectively, and z_1 is the height of the lowest model level. The sensible heat flux in the lowest layer was defined as:

$$F_{h1} = -K_{h1} \frac{\theta_v(z_2) - \theta_v(z_1)}{\Delta z_1}, \tag{17}$$

where K_{h1} denotes the vertical eddy diffusivity for heat in the lowest model layer estimated from the surface layer theory as in Eq. (16) and Δz_1 represents the thickness of the lowest model layer. Combining Eq. (17) and Eq. (18), the convective mixing rate can be calculated as:

$$M = \frac{K_{h1}}{(h - z_1)\Delta z_1}. \tag{18}$$

3.3. Determination of the ABL height

The height of the ABL, one of the mean characteristics of the boundary layer, shows a strong diurnal variation. The model determines the ABL height by specifying a critical value of the bulk Richardson number (Ri_b), defined by:

$$h = Ri_b \frac{u(h)^2 + v(h)^2}{\beta\left[\theta_v(h) - \theta_s\right]}, \tag{19}$$

where $u(h)$ and $v(h)$ are the horizontal wind velocity components at h, $\theta_v(h)$ is the virtual potential temperature at h, and θ_S is an appropriate temperature of air near the surface. The near surface potential temperature (θ_S) is calculated as (*Troen* and *Mahrt*, 1986):

$$\theta_s = \theta_v(z_1) + b\frac{\left(\overline{w'\theta_v'}\right)_0}{w_m}, \tag{20}$$

where b is a semi-empirical constant (b = 8.5, *Holtslag et al.*, 1990). The top of the ABL is diagnosed as the height where the bulk Richardson number is equal to the critical Richardson number.

4. Model evaluation

Model evaluation plays an important role in model development. A good ABL model should be able to predict realistic vertical profiles of temperature, humidity, and winds, as well as simulate the morning growth, maximum height, and evening collapse of the boundary layer. During the evaluation process, our model was tested by controlled offline numerical experiments, where initial conditions and forcing were specified. Furthermore, the model tests were performed using the Wangara observational data. The model runs were done with equally spaced vertical layers in z coordinates. Stability was defined by the surface layer bulk Richardson number as: $Ri_0 > 0.01$ for stable conditions, $-0.01 \le Ri_0 \le 0.01$ for neutral static conditions, and $Ri_0 < -0.01$ for the unstable boundary layer. For the test runs, *Dyer*'s (1974) profile functions were used, and the semi empirical constant a necessary to estimate ratio between local and nonlocal mixing processes (see Eq. (12)) was set to 7.2 (*Holtslag* and *Boville*, 1993). The top of the ABL is diagnosed as the height where the bulk Richardson number is equal to the critical Richardson number, which value was set to 0.25 (*Holtslag et al.*, 1990).

4.1. Controlled offline numerical experiments

The controlled offline experiments were performed for a dry atmosphere with a defined initial potential temperature (θ) and horizontal wind (u and v) profiles. The constant potential temperature increase of the lowest model level was determined with a magnitude of 0.16 K/h (*Nieuwstadt et al.*, 1992), the roughness length was set to 0.1 m, and the geostrophic wind components were u_g = 10 m/s and v_g = 0 m/s at all levels.

The simulated potential temperature profiles after the 4th and 8ht hour of integration obtained by estimating the ratio between local and nonlocal mixing processes (R) in every time step are presented in *Fig. 4*. The vertical model resolution was 50 m. The simulated profiles show a downward gradient from the ground up to 2/3 of the ABL height. *Fig. 5* compares profiles shown in *Fig. 4* (varying R), profiles obtained assuming that during unstable conditions the local and nonlocal mixing processes are in equilibrium ($R = 1$), and profiles simulated

by the local eddy diffusivity scheme ($R \to \infty$). As expected, the defined weak forcing local mixing processes were dominant and the profiles obtained by the varying ratio between local and nonlocal mixing processes showed a more local than a nonlocal character.

Fig. 6 describes the time evolution of the ABL height simulated by different vertical model resolutions (25 m, 50 m, and 100 m) by the varying ratio between local and nonlocal mixing processes. Since weak forcing was used in the simulation, the ABL height increased slowly. The estimation of the boundary layer height was independent of vertical resolution. Performed controlled numerical experiments showed that simulated potential temperature (θ) as well as horizontal wind (u and v) profiles were also free of vertical model resolution. The profiles obtained for eastward (u) and northward (v) wind components simulated after the 4th and 8th hours of integration by varying R are presented in *Fig. 7*. Model runs were done by 50 m vertical resolution. *Fig. 8* compares the horizontal wind profiles simulated by the eddy diffusivity scheme ($R \to \infty$), constant ($R = 1$), and varying ratio between local and nonlocal processes (profiles shown in *Fig. 7*). The differences among combined closure profiles are negligible. These profiles simulate slightly higher v wind speeds in the mixed layer and slightly lower u wind speeds near the top of the ABL than profiles obtained by local closure approach.

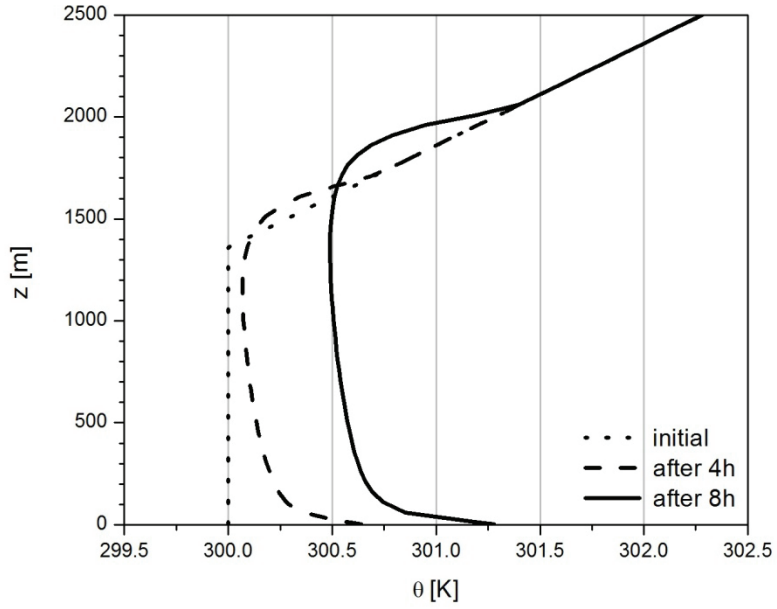

Fig. 4. Potential temperature profile at initial time and simulated after the 4th and 8th hour of integration.

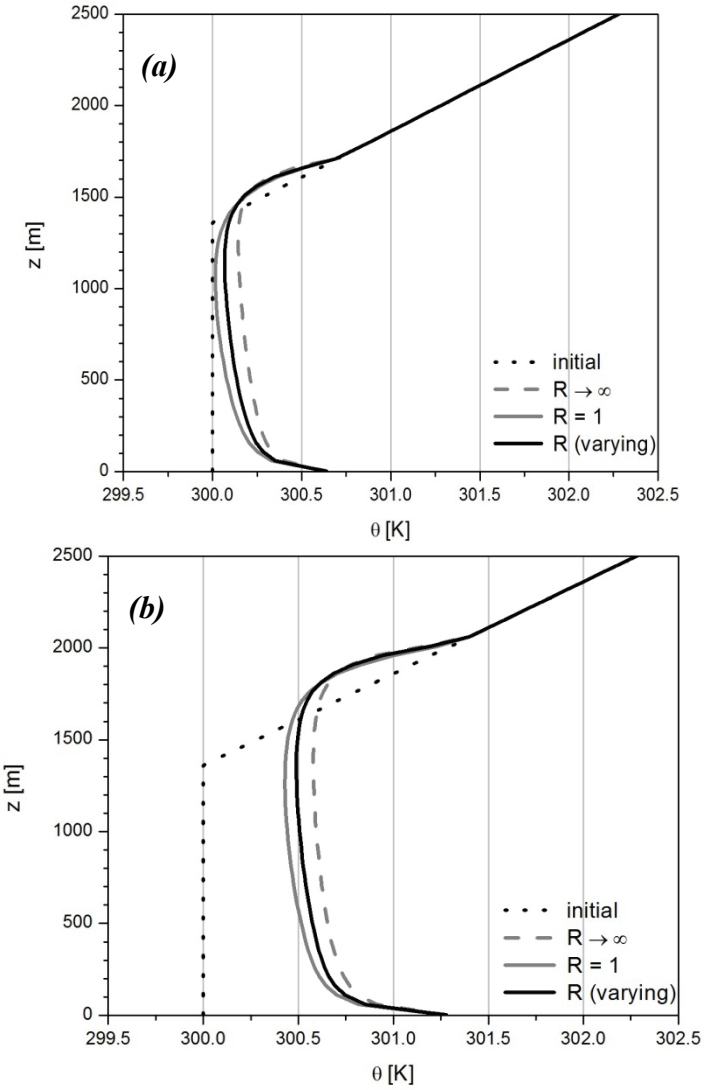

Fig. 5. Potential temperature profiles at initial time and simulated after the 4th *(a)* and 8th *(b)* hour of integration by different mixing approaches.

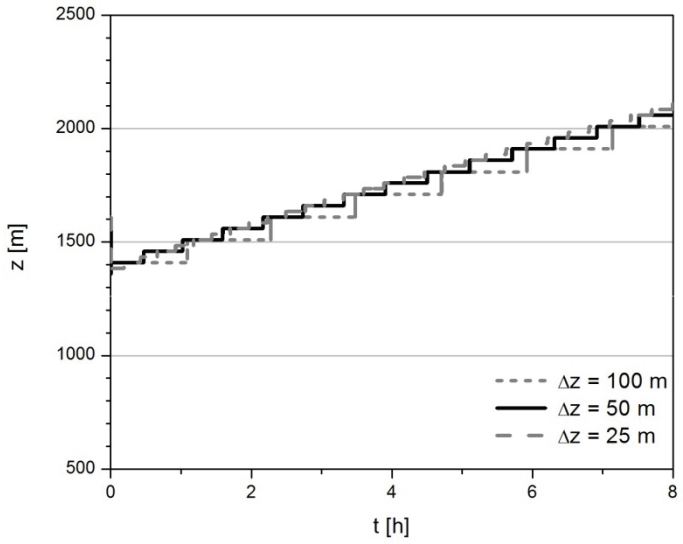

Fig. 6. Time evolution of the ABL height obtained by different vertical resolutions.

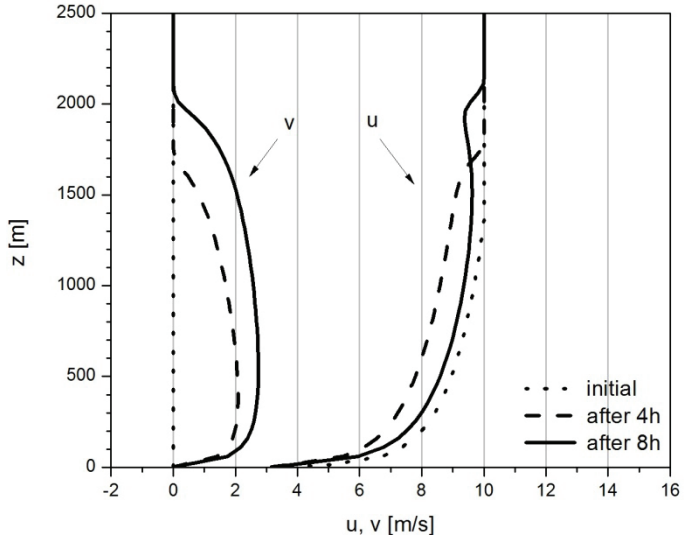

Fig. 7. Horizontal wind profiles at initial time and simulated after the 4th and 8th hour of integration.

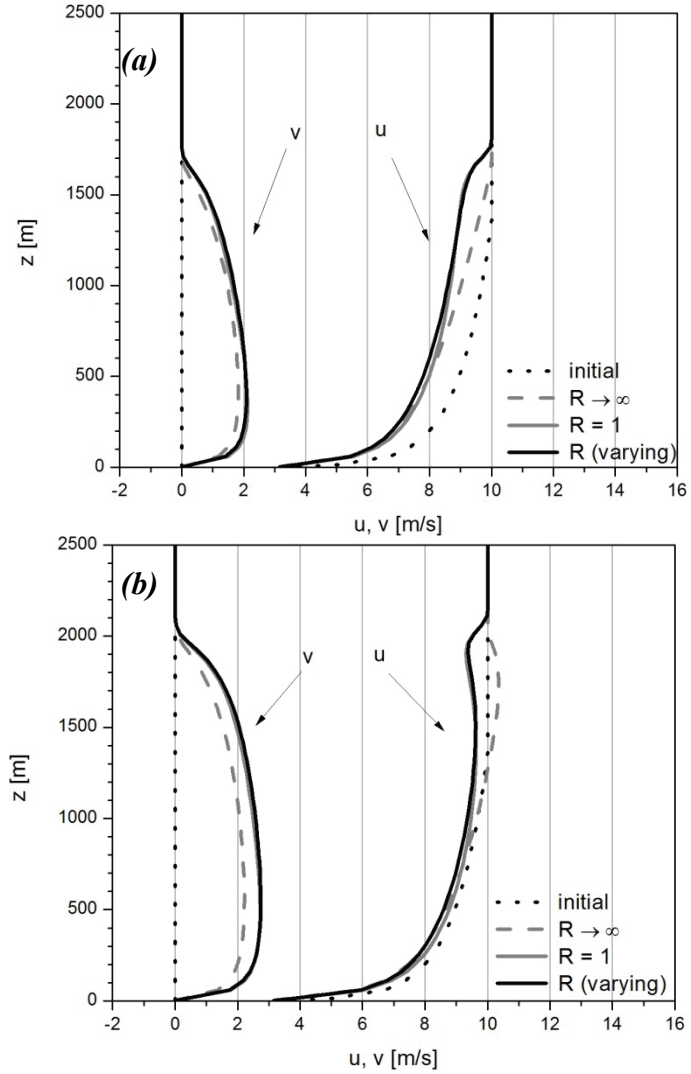

Fig. 8. Horizontal wind profiles at initial time and simulated after the 4th *(a)* and 8th *(b)* hour of integration by different mixing approaches.

4.2. Comparison with the Wangara observations

The Wangara campaign (*Clarke et al.*, 1971; *Hess et al.*, 1981) was one of the first field experiments to define the universal characteristics of the ABL. It was conducted in July and August 1967 near Hay (New South Wales, Australia). The name "Wangara" was taken from an Aboriginal word for “west wind”, which was the primary focus of the experiment. The area was selected because of its flatness, small slope, and all-weather accessibility. The observational site was located over a sparsely and uniformly vegetated region close to a desert. Over such areas, errors arising from the insufficient representation of vegetation-atmosphere interactions should be at a minimum during simulations. The high density of the observational network and the availability of many meteorological parameters (pilot balloons were released hourly, radiosonde every three hours) made the Wangara database very popular for model comparison and evaluation studies.

Our model tests were done using the data for day 33 (August 16) of the Wangara database. This particular day has been used quite often as a test case for different types of ABL models (*Yamada* and *Mellor*, 1975; *Pleim* and *Xiu*, 1995; *Alpaty et al.*, 1997; *Xue et al.*, 2001.; *Cara-Lyn et al.*, 2010) because the sky was clear the whole day and horizontal advection was very weak. Our model calculations were done by a 50 m vertical model resolution. The vertical resolution of the Wangara data is 50 m from the land surface to 1000 m, and 100 m from 1000 m to 2000 m. The initial profiles for the potential temperature (θ), water vapor mixing ratio (q), and horizontal wind components (u, v) were the observed values at 0900 LT (local time). The time variation of these quantities at the lowest model level were set explicitly as a lower boundary condition in the model. The virtual potential temperature was calculated using measured and simulated data for potential temperature and water vapor mixing ratio. According to *Yamada* and *Mellor* (1975), the roughness length was set to 0.01 m.

Observed and modeled (by varying R) virtual potential temperature profiles at four times during day 33 are shown in *Fig. 9*. The profile at 0900 LT shows a stable boundary layer. By 1200 LT, the inversion was dissipated and a convective layer was formed in both vertical profiles. The predicted top of the ABL is slightly underestimated. From 1200 LT to 1500 LT, the mean mixed layer warmed up by about 2 K. At 1800 LT, the profiles show a formed surface inversion with a well mixed residual layer.

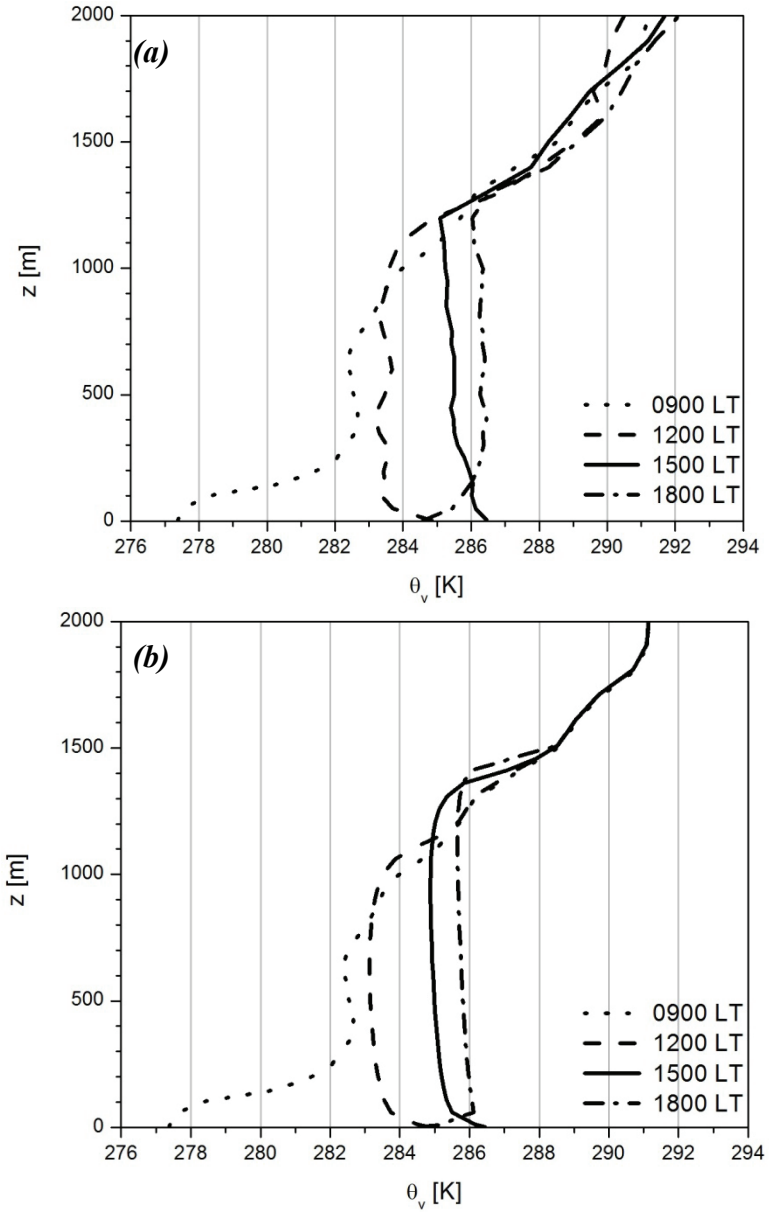

Fig. 9. The Wangara observational *(a)* and modeled *(b)* virtual potential temperature profiles.

Fig. 10 compares the virtual potential temperature profiles obtained by the eddy diffusivity scheme ($R \to \infty$), a combined mixing scheme with constant ($R = 1$), and a varying (varying R) ratio between mixing processes at 1200 LT and 1500 LT. The predicted profiles for 1200 LT are very close to the observations. At lower altitudes it is the combined closure profiles, while near the top of the boundary layer it is the local closure profile that fit the Wangara data better. The differences between the simulated and observed profiles for 1500 LT are higher. In the lower part of the boundary layer, the best fit was obtained by the local closure profile. The combined closure profiles, on the other hand, estimate the height of the boundary layer better.

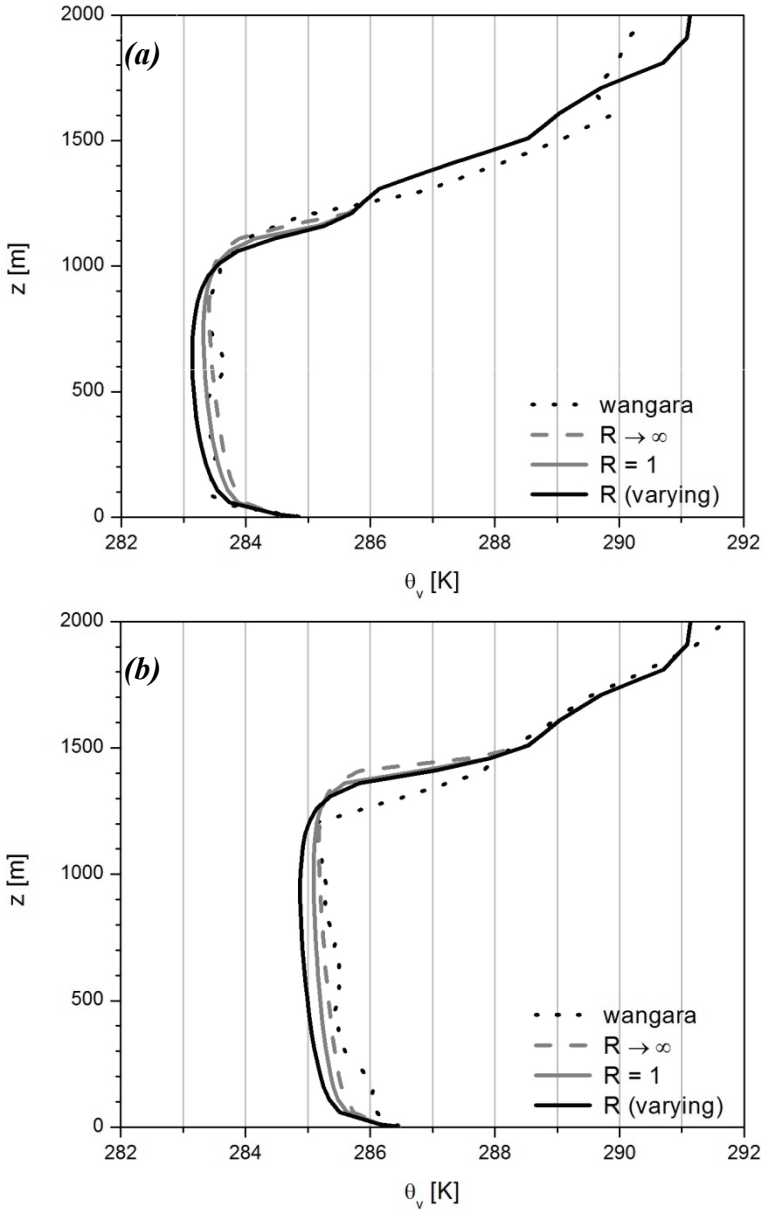

Fig. 10. Comparison of simulated and observational virtual temperature profiles at 1200 LT *(a)* and 1500 LT *(b)*.

The observed and modeled ABL heights are presented in *Fig. 11*. The observations were estimated using two methods from radiosonde measurements: as reported by *Yamada* and *Mellor* (1975), and by applying the determination process described in Section 3.3. The time resolution of the three ($R \to \infty$, $R = 1$, and varying R) modeled ABL heights is one hour. The modeled and observed heights agree very well in timing of rise, and they also predict the collapse of the ABL. At 1800 LT, when the ground-based inversion was developed, the first observational method actually represents the top of the residual layer.

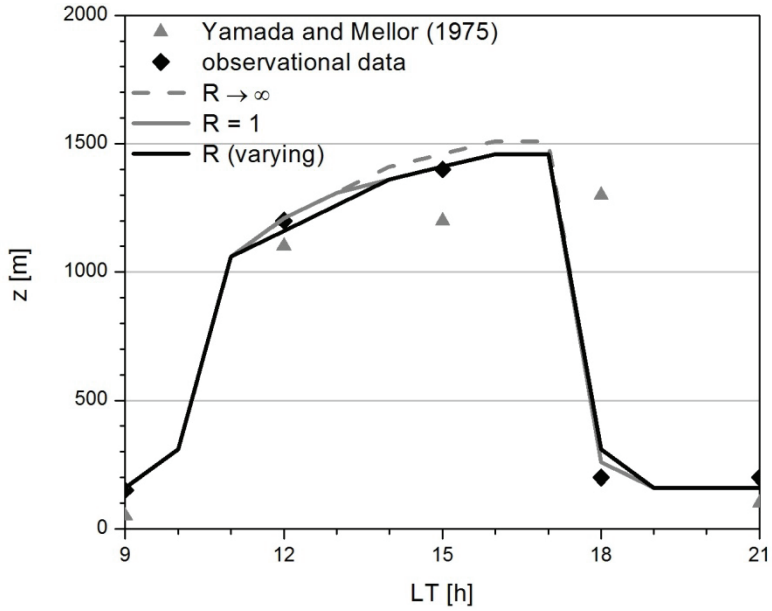

Fig. 11. Temporal evolution of the estimated and predicted height of the ABL for the Wangara simulation.

Fig. 12 compares the observed and the three predicted ($R \to \infty$, $R = 1$, and varying R) horizontal wind profiles at 1200 LT and 1800 LT. Geostrophic wind profiles were estimated from a parabolic fit to the thermal wind data as suggested by *Yamada* and *Mellor* (1975). As a function of height and time, the resulting geostrophic winds were supplied to the model as input. The differences between the modeled profiles are very small, with the highest difference being approximately 0.5 m/s. These profiles show similar features to the observations. For 1200 LT, the v profiles fit well, while the u profiles underestimate the observational data. Underestimation is explicit from 800 m to the top of the boundary layer at 1150 m. The predicted winds at 1800 LT are close to the observations. The simulated u profiles slightly underestimate, while v profiles at lower altitudes overestimate the measured data. The average difference between the estimated and measured values is about 1 m/s. The differences between the observed and simulated profiles may be due to the uncertainty in geostrophic wind estimation (*Yamada* and *Mellor*, 1975).

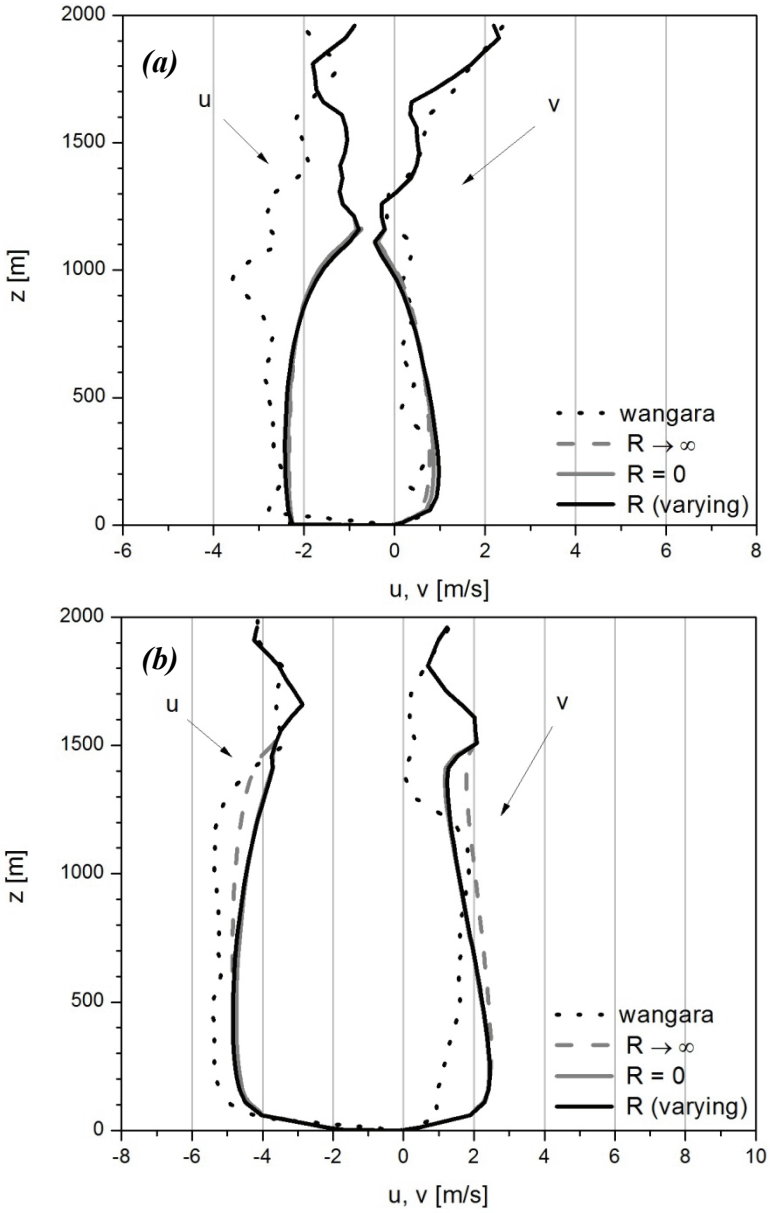

Fig. 12. Observed and simulated horizontal wind profiles at 1200 LT *(a)* and 1800 LT *(b)*.

5. Summary

This paper presents a first order single-column (1D) ABL model with a combined closure approach. In order to describe ABL properties as accurately as possible, the model calculates the local to nonlocal mixing ratio in every time step. According to the current ratio, the model simulates the turbulent mixing of prognostic variables as a split between small scale and large scale components. The obtained mixing ratio values verify the combined character of the turbulent mixing during unstable conditions. It was also proven that the uncertainty range caused by the choice of profile function types does not have a significant bearing on the obtained results.

In order to verify the validity of the model, controlled offline numerical experiments were conducted. These experiments showed that the designed model is able to simulate realistic potential temperature and wind profiles, and indicate differences among local and combined closure. A comparison with the Wangara Experiment data demonstrated a good agreement between the measured and simulated vertical profiles and it also provided a reasonably accurate estimation of the ABL height during the temporal evolution and collapse. The next step in our work is to incorporate the presented single column model into the WRF model and compare the obtained model outputs with other first and higher order profiles simulated in 1D and 3D environments.

Acknowledgements: The authors thank the European Union and the European Social Fund for their financial support (grant agreement no. TÁMOP-4.2.1.B-11/2/KMR-2011-0001 "Critical infrastructure defense research") during the preparation of this paper. The financial support of the Hungarian Scientific Research Foundation (OTKA, project no. K83909, and no. NN109679) is also greatly appreciated.

References

Ács, F. and *Kovács, M.*, 2001: The surface aerodynamic transfer parameterization method SAPA: description and performance analyses. *Időjárás 105*, 165–182.

Alapaty, K., Pleim, J.E., Raman, S., Niyogi, D.S., and *Byune, D.W.*, 1997: Simulation of atmospheric boundary layer processes using local- and nonlocal-closure schemes. *J. Appl. Meteorol. 36*, 214–233.

Arya, P.S., 2001: Introduction to micrometeorology. Academic Press, San Diego.

Berg, L.K. and *Zhong, S.*, 2005: Sensitivity of MM5-simulated boundary layer characteristics to turbulence parameterizations. *J. Appl. Meteorol. 44*, 1467–1483.

Blackadar, A. K., 1978: Modeling pollutant transfer during daytime convection. 4th Symposium on Atmospheric Turbulence, Diffusion and Air Quality. Reno, NV, USA, 443–447.

Bordás, Á., 2008: One-column vertical turbulent mixing model for the atmospheric convective layer. *Phys. Scr. T132*, 5.

Bosveld, F.C., Baas, P., Steeneveld, G.-J., Holtslag, A.A.M., Angevine, W.M., Bazile, E., de Bruijn, E.I.F., Deacu, D., Edwards, J.M., Ek, M., Larson, V.E., Pleim, J.E., Matthias Raschendorfer, M., and *Svensson, G.*, 2014: The third GABLS intercomparison case for evaluation studies of boundary-layer models. Part B: results and process understanding. *Bound.-Lay. Meteorol. 152*, 157–187.

Brown, A.R. and *Grant, A.L.M.*, 1997: Non-local mixing of momentum in the convective boundary layer a review of flux-profile relationships. *Bound.-Lay. Meteorol. 84*, 1–22.

Businger, J.A., Wyngaard, J.C., Izumi, Y., and *Bradley, E.F.*, 1971: Flux-profile relationships in the atmospheric surface layer. *J. Atmos. Sci. 28*, 181–189.

Cara-Lyn L., Randall, D., and *Yamaguchi, T.*, 2010: A higher-order closure model with an explicit PBL top. *J. Atmos. Sci. 67*, 834–850.

Clarke, R.H., Dyer, A.J., Brook, R.R., Reid, D.G., and *Troup, A.J.*, 1971: The Wangara Experiment: boundary layer data. *Tech. Paper No. 19*, CSIRO, Div. Meteor. Phys.

Dyer, A. J., 1974: A review of flux-profile relationships. *Bound.-Lay. Meteorol. 7*, 363–372.

Dyer, A.F. and *Bradley, E.F.*, 1982: An alternative analysis of flux-gradient relationships at the 1967 ITCE. *Bound.-Lay. Meteorol. 22*, 3–19.

Fiedler, B.H. and *Moeng, C.-H.*, 1985: A practical integral closure model for mean vertical transport of a scalar in a convective boundary layer. *J. Atmos. Sci. 42*, 359–363.

Foken, T., 2006: Angewandte Meteorologie, Mikrometeorologische Methoden. Springer, Heidelberg.

Frech, M. and *Mahrt, L.*, 1995: A two-scale mixing formulation for the atmospheric boundary layer. *Bound.-Lay. Meteorol. 73*, 91–104.

Hess, G.D., Hicks, B.B., and *Yamada, T.*, 1981: The impact of the Wangara Experiment. *Bound.-Lay. Meteorol. 20*, 135–174.

Holtslag, A.A.M. and *Boville, B.A.*, 1993: Local versus nonlocal boundary-layer diffusion in a global climate model. *J. Climate 6*, 1825–1842.

Holtslag, A.A.M., De Bruin, E.I.F., and *Pan, H.-L.*, 1990: A high resolution air mass transformation model for short-range weather forecasting. *Mon. Weather Rev. 118*, 1561–1575.

Hong, S.-Y., Noh, Y., and *Dudhia, J.*, 2006: A new vertical diffusion package with an explicit treatment of entrainment process. *Mon. Weather Rev. 134*, 2318–2341.

Hu, X.-M., Nielsen-Gammon, J.W., and *Zhang, F.*, 2010: Evaluation of three boundary layer schemes in the WRF model. *J. Appl. Metorolol Climate 49*, 1831–1844.

Kleczek, M.A., Steeneveld, G.-J., and *Holtslag, A.A.M.*, 2014: Evaluation of the Weather Research and Forecasting mesoscale model for GABLS3: impact of boundary-layer schemes, boundary conditions and spin-up. *Bound.-Lay. Meteorol. 152*, 213–243.

Kramm, G., Amaya, D.J., Foken, T., and *Mölders, N.*, 2013: Hans A. Panofsky's Integral Similarity Function – At Fifty, *Atmos. Climate Sci. 3*, 581–594.

Noh, Y., Cheon, W.G., Hong, S.Y., and *Raasch, S.*, 2003: Improvement of the K-profile model for the planetary boundary layer based on large eddy simulation data. *Bound.-Lay. Meteorol. 107*, 401–427.

Nieuwstadt, F.T.M., Mason, P.J., Moeng, C.-H., and *Schumann, U.*, 1992: Large Eddy Simulations of the Convective Boundary Layer: A Comparison of Four Computer Codes. In Turbulent Shear Flows Vol. 8, Springer, 343–367.

Pleim, J.E., 2007a: A combined local and nonlocal closure model for the atmospheric boundary layer. Part I: model decription and testing. *J. Appl. Metorol. Climate 46*, 1383–1395.

Pleim, J.E., 2007b: A combined local and nonlocal closure model for the atmospheric boundary layer. Part II: application and evaluation in a mesoscale meteorological model. *J. Appl. Metorol. Climate 46*, 1396–1409.

Pleim, J.E. and *Chang, J.S.*, 1992: A non-local closure model for vertical mixing in the convective boundary layer. *Atmos. Environ. 26A*, 965–981.

Pleim, J.E. and *Xiu, A.*, 1995: Development and testing of a surface flux and planetary boundary layer model for application in mesoscale models. *J. Appl. Meteorol. 34*, 16–34.

Shin, H.H. and *Hong, S.–Y.*, 2011: Intercomparison of Planetary Boundary-Layer Parametrizations in the WRF Model for a Single Day from CASES-99. *Bound.-Lay. Meteorol. 139*, 261–281.

Stull, R.B., 1984: Transilient tubulence theory. Part I: The concept of eddy-mixing across finite distances. *J. Atmos. Sci. 41*, 3351–3367.

Stull, R.B., 1988: An introduction to Boundary layer meteorology. Kluwer Academic Publ., Dordrecht.

Troen, I.B. and *Mahrt, L.*, 1986: A simple model of the atmospheric boundary layer; sensitivity to surface evaporation. *Bound.-Lay. Meteorol. 37*, 129–148.

Weidinger, T., Pinto, J., and *Hotváth, L.*, 2000: Effects of uncertainties in universal functions, roughness length, and displacement height on the calculation of surface layer fluxes. *Meterorol. Z. 9*, 139–154.

Xie, B., Fung, J.C.H, Chan, A., and *Lau, A.*, 2012: Evaluation of nonlocal and local planetary boundary layer schemes in the WRF model. *J. Geophys. Res. 117*, D12103.

Xue, M., Droegemeier, K. K., Wong, V., Shapiro, A., Brewster, K., Carr, F., Weber, D., Liu, Y., and *Wang, D.*, 2001: The advanced regional prediction system (ARPS) – a multi-scale nonhydrostatic atmospheric simulation and prediction tool. Part II: model physics and applications. *Meteorol. Atmos. Phys. 76*, 143–165.

Yamada, T. and *Mellor, G.*, 1975: A simulation of the Wangara atmospheric boundary layer data. *J. Atom. Sci. 32*, 23099–2329.

Zilitinkevich, S.S. and *Chalikov, D.V.*, 1968. Determining the universal wind-velocity and temperature profiles in the atmospheric boundary layer. *Izv. Atmospheric and Oceanic Physics 4*, 2949–302. (English version 1659–170.)

Zhang, D. and *Anthes, R.A.*, 1982: A high-resolution model of the planetary layer – sensitivity tests and comparison with SESAME-79 data. *J. Appl. Meteor. 21*, 1594–1609.

Zhang, D.L. and *Zheng, W.Z.*, 2004: Diurnal cycles of surface winds and temperatures as simulated by five boundary layer parameterizations, *J. Appl. Meteor. 43*, 157–169.